ACS Sustainable Chemistry & Engineering

pubs.acs.org/journal/ascecg

Research Article

Computational Mechanism of Methyl Levulinate Conversion to γ-Valerolactone on UiO-66 Metal Organic Frameworks

Manuel A. Ortuño,* Marcos Rellán-Piñeiro, and Rafael Luque

Cite This: *ACS Sustainable Chem. Eng.* 2022, 10, 3567−3573

Read Online

ACCESS | Metrics & More | Article Recommendations | Supporting Information

ABSTRACT: Metal−organic frameworks (MOFs) are gaining importance in the field of biomass conversion and valorization due to their porosity, well-defined active sites, and broad tunability. But for a proper catalyst design, we first need detailed insight of the system at the atomic level. Herein, we present the reaction mechanism of methyl levulinate to γ-valerolactone on Zr-based UiO-66 by means of periodic density functional theory (DFT). We demonstrate the role of Zr-based nodes in the catalytic transfer hydrogenation (CTH) and cyclization steps. From there, we perform a computational screening to reveal key catalyst modifications to improve the process, such as node doping and linker exchange.

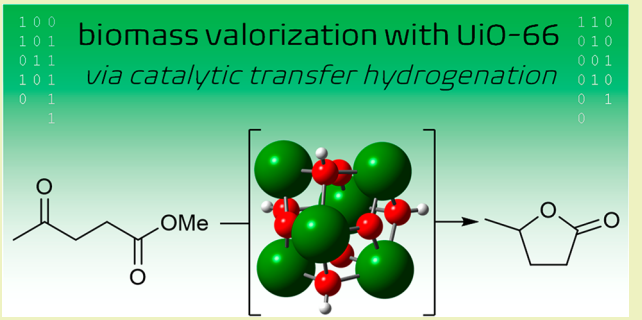

KEYWORDS: *Density functional theory (DFT), Metal organic framework (MOF), Catalyst design, Biomass valorization, Catalytic transfer hydrogenation (CTH)*

INTRODUCTION

The current scenario dominated by crude oil and natural gas is no longer feasible, and our society needs to devise new sustainable ways to fulfill the feedstock demand of an increasing world population. We must abandon the limited supply of fossil fuels and turn to renewable resources such as biomass. Indeed, the upgrading of readily available lignin and (hemi)cellulose to high-value products is already leading the way toward a sustainable economy.[1] In that regard, several biobased molecules have been identified as promising building blocks.[2] Among them, we here target the transformation of methyl levulinate (ML), readily available from lignocellulose, into γ-valerolactone (GVL), a platform molecule used as solvent, fuel, and feedstock for high-value chemicals.[3]

This reaction is typically catalyzed in the heterogeneous phase and entails a direct hydrogenation via precious metals.[4] Alternatively, amphoteric catalysts, such as those based on Zr, can promote a catalytic transfer hydrogenation (CTH) using alcohols as a hydrogen source (Scheme 1),[5,6] thus avoiding the need of hydrogen gas and expensive metals. Zr-based oxides can indeed promote this process,[7,8] but the variety of active sites on the catalyst surface may become detrimental due to undesired side reactions.

Scheme 1. Conversion of Methyl Levulinate (ML) into γ-Valerolactone (GVL) via Catalytic Transfer Hydrogenation

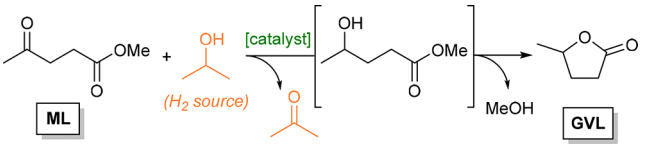

To better control the design of catalytic sites, we turn to metal−organic frameworks (MOFs), a family of porous materials that comprises inorganic nodes connected through organic linkers.[9] Their high surface area, variable porosity, and well-defined coordination modes make them very valuable for general catalytic applications.[10] This scope has been expanded to biomass conversion in recent years.[11,12] Due to the thermal stability and catalytic properties of MOFs containing Zr_6O_8 nodes (Figure 1),[13] they were tested in the valorization of alkyl levulinates to GVL via CTH. UiO-66 exhibited high activity and selectivity toward GVL in both batch[14] and flow[15] setups. Interestingly, while NH_2- and COOH-functionalized linkers did not improve the catalytic performance,[14] the presence of SO_3H groups had a positive impact, presumably due to a cooperative effect between Lewis base nodes and Brønsted acid linkers.[16] Other MOFs with similar Zr_6O_8 nodes (MOF-808,[14] DUT-52,[17] and ZrF[18]) can also catalyze this reaction with high conversion and moderate-to-good selectivity, as well as some Hf-based analogues.[19] The improved catalytic activity obtained

Received: November 26, 2021
Revised: February 24, 2022
Published: March 4, 2022

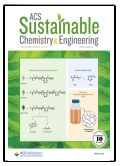

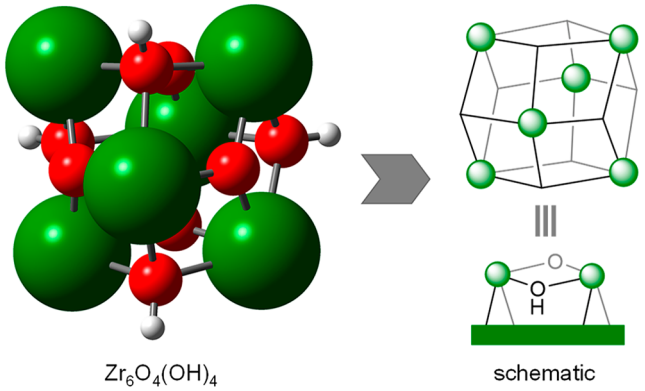

Figure 1. Representation of Zr-based nodes. Zr = dark green, O = red, H = white.

by MOF tuning is general and can be extrapolated to other processes, as recently demonstrated in UiO-66-catalyzed carbohydrate conversion.[20]

These promising results encourage further mechanistic understanding for catalyst optimization. Here is where computational chemistry comes into play to provide quantum mechanical insight at the atomic level of detail.[21] Despite the many computational contributions on MOF catalysis,[22,23] the mechanistic features of how these materials participate in biomass valorization are still scarce. Most of these studies employ finite-size clusters,[24] which ignore the periodicity of the material and cannot account for confinement effects within the pores. To address this gap in knowledge, here we employ periodic density functional theory (DFT) to create a more realistic environment. We compute the reaction mechanism of ML to GVL at UiO-66 using isopropanol as a hydrogen source. We identify the key steps of the catalytic cycle and evaluate the impact of different catalyst modifications. Such mechanistic insight would guide the rational design of catalysts to develop more efficient and selective experimental systems.

COMPUTATIONAL SECTION

Calculations were performed at the periodic Density Functional Theory (DFT) level using the Vienna Ab-Initio Simulation Package (VASP).[25,26] The PBE density functional[27] was employed, and dispersion interactions were considered with Grimme's D2 scheme.[28] Core electrons were described by projector augmented wave (PAW) pseudopotentials,[29] and valence electrons were represented by plane waves with a kinetic energy cutoff of 450 eV. A Hubbard correction[30] of 4.5 eV was applied to Ce(4f) electrons as suggested in the literature.[31,32] The simulation cell of UiO-66 (14.737 × 20.840 × 14.737 Å^3, Figure S1) was taken from previous DFT calculations.[33] The Brillouin zone was sampled at the Γ-point via the Monkhorst−Pack method.[34] Transition state structures were located with the climbing image nudged elastic band[35] and improved dimer[36] algorithms. Minima and transition states were characterized by diagonalizing the numerical Hessian matrix (±0.015 Å displacements). Vibrational partition functions were computed using numerical frequencies at 513 K as in experiments,[15] where only selected atoms were allowed to move.[37]

Open access[38] to all inputs and outputs reported herein, including raw energies and geometries, is provided by the ioChem-BD platform[39] in the following database.[40]

RESULTS AND DISCUSSION

The UiO-66 MOF is formed by $Zr_6O_4(OH)_4$ nodes connected to 12 1,4-benzenedicarboxylate linkers.[41] The pristine material does not have any open metal sites, but the presence of defects, i.e., missing linkers, is known to be responsible for catalytic activity.[42,43] Thus, we first need to propose a feasible active site where the ML-to-GVL conversion may take place.

The unit cell of UiO-66 contains four inorganic nodes.[41] To save computational resources, we use a smaller cell containing two inorganic nodes.[33] The removal of one dicarboxylate linker creates two node defects with four metal vacancies overall, which we then balance with OH/H_2O groups.[44] Under reaction conditions, we expect a displacement of H_2O and exchange of $[OH]^-$ by $[^iPrO]^-$, yielding the potential active species **1** (Figure 2). We will use this structure as a starting point for computing the reaction mechanism.

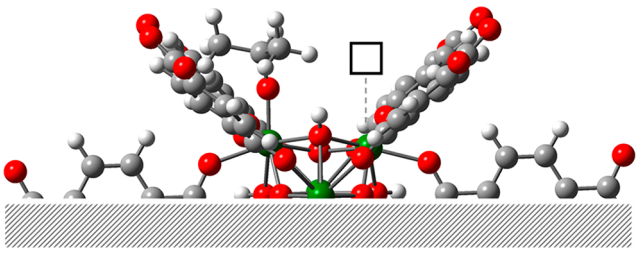

Figure 2. Computed structure **1** at defective UiO-66 MOF. The periodic structure was cropped for better visualization. The black square indicates a Zr vacant site. Zr = dark green, O = red, H = white.

Reaction Mechanism at Defective UiO-66. We start the mechanistic study from the previously discussed structure **1** which contains one ^{i}PrO group and one Zr vacant site. We establish this stage as the zero of energies. The following values correspond to Gibbs energies computed at 513 K in eV. All species are denoted with numbers in bold, where transition states include the prefix **TS**.

The proposed reaction mechanism is depicted in Figure 3 and entails catalytic transfer hydrogenation of ML followed by cyclization to GVL. First, species **1** binds ML through its carbonyl group forming **2** (0.14 eV). The hydrogen transfer from ^{i}PrO to the activated ML occurs via **TS2−3** (0.61 eV) involving two Zr centers[45] and yields intermediate **3** (0.39 eV). From there, acetone is released via **4** (−0.09 eV) and the alkoxide rearranges to form the bidentate species **5** (−0.51 eV), where the ester carbonyl group is also bound to Zr. An intramolecular nucleophilic attack via **TS5−6** (0.13 eV) generates the intermediate **6** (−0.14 eV). The subsequent elimination of MeOH is assisted by the μ_3-OH group of the node.[46−48] It takes place via **TS6−7** (0.15 eV) and results in the formation of bounded GVL in **7** (−0.35 eV). The nonassisted elimination via **TS6−8** (0.46 eV), which yields the Zr−OMe intermediate **8**, is less favored (Figure S2). Finally, an incoming ^{i}PrOH reactant molecule releases the GVL product and regenerates catalyst **1**. The computed mechanism is in line with the experimental proposal, which involves two Zr atoms from the same node[14] (rather than two Zr atoms from adjacent nodes[16]).

The Gibbs energy profile of the reaction mechanism catalyzed by defective UiO-66 is displayed in Figure 4 (the electronic energy profile can be found in Figure S3). The coordination of ML to the catalyst **1** is slightly uphill by 0.14

https://doi.org/10.1021/acssuschemeng.1c08021
ACS Sustainable Chem. Eng. 2022, 10, 3567−3573

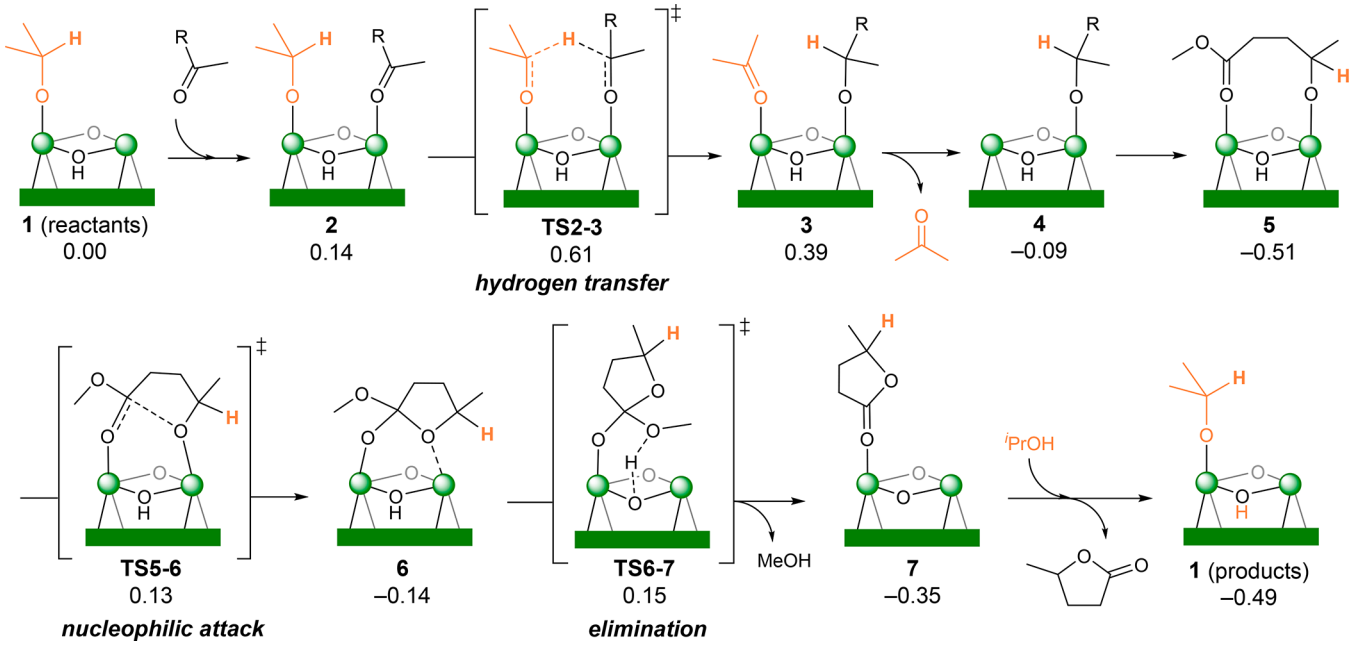

Figure 3. Reaction mechanism of ML to GVL at defective UiO-66 with relative Gibbs energies (in eV). R = $(CH_2)_2CO_2Me$.

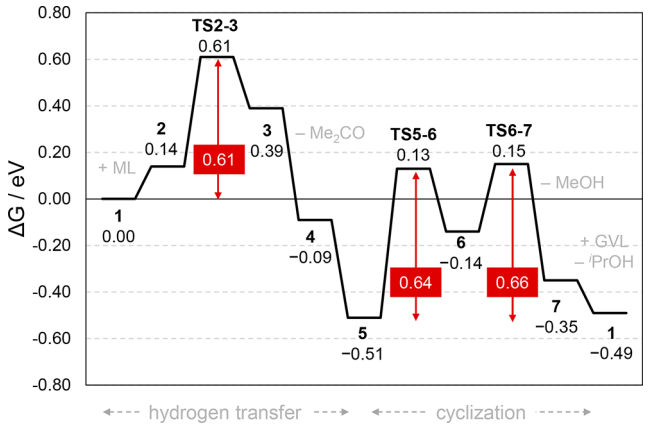

Figure 4. Gibbs energy reaction profile (in eV) at defective UiO-66 with relative barriers for each step.

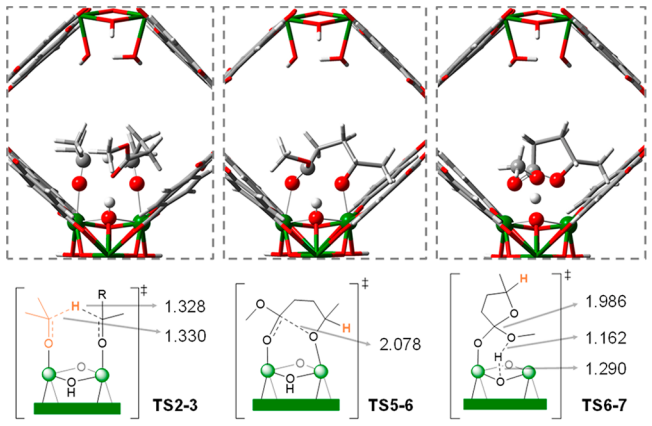

Figure 5. DFT-optimized TS structures. Relevant atoms are display in ball-and-stick format, the rest of them in tube format. Selected distances are shown in Å.

eV, but this step is temperature-sensitive, and computed Gibbs energies typically over stabilize separated reactants due to entropic contributions. The hydrogen transfer **TS2−3** has a barrier of 0.61 eV above **1** and a relative barrier of 0.47 eV above **2**. Similar values were recently found in the CTH of furfural to furfuryl alcohol using finite-size cluster models of UiO-66[49] and MOF-808.[50] The release of acetone followed by the bidentate coordination of the substrate is quite favored, with **5** at 0.51 eV below **1**. Next, the cyclization takes place via nucleophilic attack and elimination of MeOH, where both **TS5−6** and **TS6−7** present similar barriers of 0.64 and 0.66 eV above **5**, respectively. The release of GVL and the addition of ^{i}PrOH recover the catalyst **1** with global exoergic thermodynamics of 0.49 eV.

The structures of selected transition states confined within the MOF pore are displayed in Figure 5. **TS2−3** shows the hydrogen transfer; also, the ester group of ML forms a H bond with the μ_3-OH group. **TS5−6** describes the intramolecular attack of the alkoxy to the carbonyl group. Finally, **TS6−7** represents the departure of the methoxy group and the concomitant abstraction of a proton from the μ_3-OH group of the node. Further simulations at the PBE level with and without D2 dispersion corrections demonstrate the importance of such confinement effects (Figure S4), with **TS2−3** (hydrogen transfer) more affected than **TS5−6** and **TS6−7** (cyclization).

These simulations predict overall Gibbs energy barriers of ca. 0.65 eV for the UiO-66 catalyst. It demonstrates that the proposed mechanism is feasible under the reported experimental conditions, either in batch[14,16] or flow reactors.[15] They also predict that the cyclization process is likely rate-determining, which is in line with the detection of slight amounts of methyl 4-hydroxypentanoate.[15,16] Due to the importance of the node in the mechanism, we next evaluate several MOF modifications that directly impact the Zr_6O_8 core: changing the nature of the metals (tuning the node) and changing the ligands bound to them (tuning the linker).

To facilitate future reading and comparison, from now on we will label all species of the original unmodified UiO-66 with the

https://doi.org/10.1021/acssuschemeng.1c08021
ACS Sustainable Chem. Eng. 2022, 10, 3567−3573

prefix **A** (e.g., **A-1**). We will use letters in bold for different modifications together with numbers in bold for intermediates and transition states. The correspondence between letters and modifications will be indicated in the following sections. The numeric notation does not change, and the correspondence between numbers and structures can be consulted in Figure 3.

Tuning the Node. The previous reaction mechanism shows that Zr atoms efficiently act as Lewis acids for carbonyl groups. We then consider whether other M(IV) atoms (Hf, Ti, and Ce) can facilitate the reaction. Although such doping is not trivial from an experimental point of view, mixed-metal nodes[51,52] and Ce-based nodes[53] have been previously reported in the literature.

Considering the two Zr atoms involved in the process (**A**), we exchange them by Hf, Ti, and Ce (**B**–**J**) as shown in Figure 6a. We then compute energy barriers for each step: hydrogen

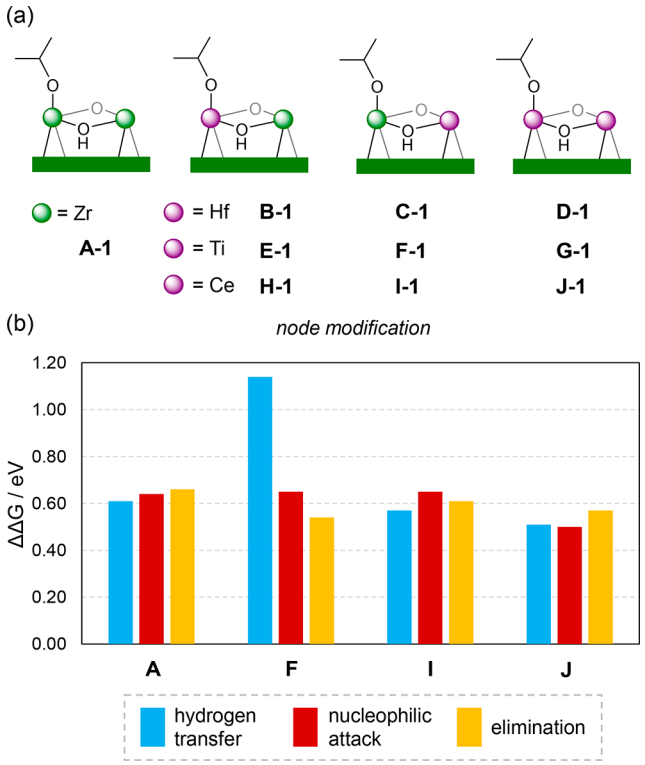

Figure 6. (a) Hf-, Ti-, and Ce-doped nodes and (b) relative Gibbs energy barriers (in eV) for selected models. Barriers are computed from the transition state to the previous most stable intermediate.

transfer (from **1** to **TS2**–**3**), nucleophilic attack (from **5** to **TS5**–**6**), and elimination (from **5** to **TS6**–**7**). For the Hf derivatives **B**–**D**, the differences in electronic energy with respect to **A** are less than 0.05 eV (Figure S5), and we expect similar Gibbs energy profiles for both Zr- and Hf-based nodes. However, more changes are noted for Ti and Ce derivatives, and representative systems are shown in Figure 6b. For **F** with one Ti, the hydrogen transfer is significantly more demanding (**F-TS2**–**3** at 1.14 eV) due to a weak adsorption of ML (**F-2** at 0.50 eV), while the nucleophilic attack remains roughly the same and the elimination becomes easier (**F-TS6**–**7** at 0.38 eV, 0.54 eV above **F-5**). For **I** with one Ce, the hydrogen transfer and elimination steps are only marginally better, and the nucleophilic attack does not change. Interestingly, for **J**, which includes two Ce atoms, all barriers are reduced. The adsorption of ML is slightly stronger (**J-2** at −0.10 eV), and the hydrogen transfer barrier is lower (**J-TS2**–**3** at 0.41 eV, 0.51 eV above **J-2**). Likewise, the alkoxy intermediate is more stable and the cyclization process is overall faster.

To sum up, the presence of Ti can speed up the cyclization process at the expense of slowing down the hydrogen transfer. Ce-containing nodes provide a general decrease of barriers for all steps, in line with simulations on chemical warfare decomposition.[54] With these results, we hypothesize that rare-earth-based MOFs[55] could also exhibit similar or improved catalytic activity for biomass-related processes.

Tuning the Linker. Not only nodes but also linkers can be fine-tuned in MOF catalysts. Therefore, we now consider changing the groups around the metals through linker modifications. Previous theoretical studies have pointed out that functionalizing the aromatic linkers has little effect on computed energy barriers[46,56] and frequencies.[57] We thus take a different approach and change the type of connectivity between the linker and the node.

As mentioned before, the unmodified MOF is labeled with the prefix **A**, where L is the original benzenedicarboylate (bdc). Considering the linkers bound to the participating Zr atoms, we exchange them by L^a and L^b as shown in Figure 7a. In L^a,

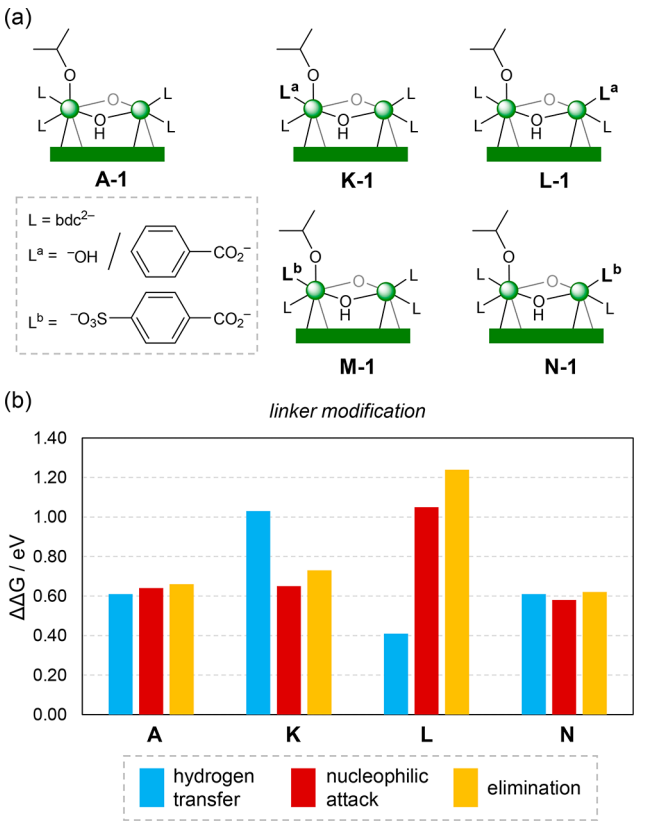

Figure 7. (a) Linker-modified nodes and (b) relative Gibbs energy barriers (in eV) for selected models. Barriers are computed from the transition state to the previous most stable intermediate.

one bidentate carboxylate group is removed, and one monodentate hydroxo is bound to Zr (**K** and **L**), thus formally introducing a new vacant site at the node. In L^b, one carboxylate group is substitute by one sulfonate group[58] (**M** and **N**). The relative Gibbs energy barriers are summarized in Figure 7b. For **K**, the adsorption of ML does not change much

https://doi.org/10.1021/acssuschemeng.1c08021
ACS Sustainable Chem. Eng. 2022, 10, 3567−3573

(**K-2** at 0.25 eV) but the hydrogen transfer becomes more difficult (**K-TS2−3** at 1.03 eV). This is due to a stronger interaction between the ^{i}PrO and the unsaturated Zr, which decreases the nucleophilicity of the former. On the other hand, for **L**, the adsorption of ML is enhanced at the unsaturated Zr (**L-2** at −0.39 eV), and the hydrogen transfer becomes faster (**L-TS2−3** at 0.41 eV above **L-2**). Although an electron deficient Zr is beneficial in the first step, it later binds to the alkoxy intermediate strongly (**L-5** at −1.57 eV), creating a thermodynamic sink that hinders the cyclization process. For **M** and **N**, both systems behave the same, and only **N** is discussed for simplicity. The sulfonate group in **N** does not introduce large changes, *cf.* the carboxylate group in **A**, and similar barriers are obtained in both cases.

Overall, these results indicate that the excess of vacancies at Zr atoms is counterproductive for activity, which may relate to the worse catalytic performance after losing organic linkers.[15] They also suggest that the reaction is feasible with MOFs containing SO_3-modified linkers. Although there is no strong improvement in terms of computed reaction barriers, these materials may present other advantages from a practical point of view, such as higher number of defects along the framework (i.e., more catalytic sites) while increasing the stability of the material, as reported recently.[58]

CONCLUSIONS

In this work, we study the role of UiO-66 in the conversion of methyl levulinate to γ-valerolactone using isopropanol as a hydrogen source. By means of periodic DFT simulations, we propose a feasible reaction mechanism in agreement with experiments, which consists of transfer hydrogenation and cyclization (nucleophilic attack followed by elimination). We find similar Gibbs energy barriers for all steps, thus no unique rate-determining step can be ascribed. Notably, the μ_3-OH group at the node actively participates in the reaction by forming H-bonds with reactants and assisting in the elimination process.

As for design, we explore several catalysts by systematically varying the metal atoms in the node as well as the connecting group between the linker and the node. Our computational approach provides a precise control of MOF changes that allows us to inspect the impact of each modification on each step of the mechanism. In this way, we demonstrate that Ti (a hard Lewis acid) improves the hydrogen transfer but is detrimental for the cyclization, while highly unsaturated Zr operates the other way around. We also find that Ce-based nodes decrease all three reaction barriers and exploring related MOFs containing rare-earth elements would be interesting. Finally, Zr nodes with SO_3-modified linkers are competitive, *cf.* the parent material, and can improve the overall performance of the catalytic system.

ASSOCIATED CONTENT

Supporting Information

The Supporting Information is available free of charge at https://pubs.acs.org/doi/10.1021/acssuschemeng.1c08021.

Alternative mechanism, electronic energy profile, additional energy barriers (PDF)

AUTHOR INFORMATION

Corresponding Author

Manuel A. Ortuño − *Centro Singular de Investigación en Química Biolóxica e Materiais Moleculares (CIQUS), Universidade de Santiago de Compostela, 15782 Santiago de Compostela, Spain; Institute of Chemical Research of Catalonia, ICIQ, and the Barcelona Institute of Science and Technology, BIST, 43007 Tarragona, Spain*; Email: manuelangel.ortuno@usc.es

Authors

Marcos Rellán-Piñeiro − *Centro Singular de Investigación en Química Biolóxica e Materiais Moleculares (CIQUS), Universidade de Santiago de Compostela, 15782 Santiago de Compostela, Spain*

Rafael Luque − *Departamento de Química Orgánica, Universidad de Córdoba, E-14014 Córdoba, Spain; Peoples Friendship University of Russia (RUDN University), 117198 Moscow, Russian Federation*; orcid.org/0000-0003-4190-1916

Complete contact information is available at: https://pubs.acs.org/10.1021/acssuschemeng.1c08021

Notes

The authors declare no competing financial interest.

ACKNOWLEDGMENTS

This work has received financial support from the Beatriu de Pinós postdoctoral program of the Government of Catalonia's Secretariat for Universities and Research (2017-BP-00039), MINECO (under project PID2020-119116RA-I00), Xunta Distinguished Researcher program (ED431H 2020/21), the Xunta de Galicia (Centro singular de investigación de Galicia accreditation 2019-2022, ED431G 2019/03), and the European Union (European Regional Development Fund - ERDF). R.L. gratefully acknowledges funding from MINECO under project PID2019-109953GB-I00. The authors acknowledge CESGA ("Centro de Supercomputación de Galicia") and RES-HPC (QS-2020-3-0019 and QS-2020-3-0022) for providing generous computational resources. This publication has been supported by RUDN University Strategic Academic Leadership Program (R.L.).

REFERENCES

(1) Tuck, C. O.; Pérez, E.; Horváth, I. T.; Sheldon, R. A.; Poliakoff, M. Valorization of Biomass: Deriving more Value from Waste. *Science* **2012**, *337*, 695−699.

(2) Bozell, J. J.; Petersen, G. R. Technology Development for the Production of Biobased Products from Biorefinery Carbohydrates—The US Department of Energy's "Top 10" Revisited. *Green Chem.* **2010**, *12*, 539−554.

(3) Alonso, D. M.; Wettstein, S. G.; Dumesic, J. A. Gamma-Valerolactone, a Sustainable Platform Molecule Derived from Lignocellulosic Biomass. *Green Chem.* **2013**, *15*, 584−595.

(4) Wright, W. R. H.; Palkovits, R. Development of Heterogeneous Catalysts for the Conversion of Levulinic acid to γ-Valerolactone. *ChemSusChem* **2012**, *5*, 1657−1667.

(5) Gilkey, M. J.; Xu, B. Heterogeneous Catalytic Transfer Hydrogenation as an Effective Pathway in Biomass Upgrading. *ACS Catal.* **2016**, *6*, 1420−1436.

(6) Shivhare, A.; Kumar, A.; Srivastava, R. An Account of the Catalytic Transfer Hydrogenation and Hydrogenolysis of Carbohydrate-Derived Renewable Platform Chemicals over Non-Precious Heterogeneous Metal Catalysts. *ChemCatChem.* **2021**, *13*, 59−80.

(7) Chia, M.; Dumesic, J. A. Liquid-Phase Catalytic Transfer Hydrogenation and Cyclization of Levulinic Acid and Its Esters to γ-Valerolactone over Metal Oxide Catalysts. *Chem. Commun.* **2011**, *47*, 12233−12235.
(8) Tabanelli, T.; Paone, E.; Vásquez, P. B.; Pietropaolo, R.; Cavani, F.; Mauriello, F. Transfer Hydrogenation of Methyl and Ethyl Levulinate Promoted by a ZrO_2 Catalyst: Comparison of Batch vs Continuous Gas-Flow Conditions. *ACS Sustainable Chem. Eng.* **2019**, *7*, 9937−9947.
(9) Furukawa, H.; Cordova, K. E.; O'Keeffe, M.; Yaghi, O. M. The Chemistry and Applications of Metal-Organic Frameworks. *Science* **2013**, *341*, 1230444.
(10) Bavykina, A.; Kolobov, N.; Khan, I. S.; Bau, J. A.; Ramirez, A.; Gascon, J. Metal-Organic Frameworks in Heterogeneous Catalysis: Recent Progress, New Trends, and Future Perspectives. *Chem. Rev.* **2020**, *120*, 8468−8535.
(11) Herbst, A.; Janiak, C. MOF Catalysts in Biomass Upgrading Towards Value-Added Fine Chemicals. *CrystEngComm* **2017**, *19*, 4092−4117.
(12) Fang, R.; Dhakshinamoorthy, A.; Li, Y.; Garcia, H. Metal Organic Frameworks for Biomass Conversion. *Chem. Soc. Rev.* **2020**, *49*, 3638−3687.
(13) Rimoldi, M.; Howarth, A. J.; DeStefano, M. R.; Lin, L.; Goswami, S.; Li, P.; Hupp, J. T.; Farha, O. K. Catalytic Zirconium/Hafnium-Based Metal-Organic Frameworks. *ACS Catal.* **2017**, *7*, 997−1014.
(14) Valekar, A. H.; Cho, K.-H.; Chitale, S. K.; Hong, D.-Y.; Cha, G.-Y.; Lee, U.-H.; Hwang, D. W.; Serre, C.; Chang, J.-S.; Hwang, Y. K. Catalytic Transfer Hydrogenation of Ethyl Levulinate to γ-Valerolactone over Zirconium-Based Metal-Organic Frameworks. *Green Chem.* **2016**, *18*, 4542−4552.
(15) Ouyang, W.; Zhao, D.; Wang, Y.; Balu, A. M.; Len, C.; Luque, R. Continuous Flow Conversion of Biomass-Derived Methyl Levulinate into γ-Valerolactone Using Functional Metal Organic Frameworks. *ACS Sustainable Chem. Eng.* **2018**, *6*, 6746−6752.
(16) Kuwahara, Y.; Kango, H.; Yamashita, H. Catalytic Transfer Hydrogenation of Biomass-Derived Levulinic Acid and Its Esters to γ-Valerolactone over Sulfonic Acid-Functionalized UiO-66. *ACS Sustainable Chem. Eng.* **2017**, *5*, 1141−1152.
(17) Kurisingal, J. F.; Rachuri, Y.; Palakkal, A. S.; Pillai, R. S.; Gu, Y.; Choe, Y.; Park, D.-W. Water-Tolerant DUT-Series Metal-Organic Frameworks: A Theoretical-Experimental Study for the Chemical Fixation of CO_2 and Catalytic Transfer Hydrogenation of Ethyl Levulinate to γ-Valerolactone. *ACS Appl. Mater. Interfaces* **2019**, *11*, 41458−41471.
(18) Yun, W.-C.; Yang, M.-T.; Lin, K.-Y. A. Water-Born Zirconium-Based Metal Organic Frameworks as Green and Effective Catalysts for Catalytic Transfer Hydrogenation of Levulinic Acid to γ-Valerolactone: Critical Roles of Modulators. *J. Colloid Interface Sci.* **2019**, *543*, 52−63.
(19) Rojas-Buzo, S.; García-García, P.; Corma, A. Catalytic Transfer Hydrogenation of Biomass-Derived Carbonyls over Hafnium-Based Metal-Organic Frameworks. *ChemSusChem* **2018**, *11*, 432−438.
(20) Ronaghi, N.; Shade, D.; Moon, H. J.; Najmi, S.; Cleveland, J. W.; Walton, K. S.; France, S.; Jones, C. W. Modulation and Tuning of UiO-66 for Lewis Acid Catalyzed Carbohydrate Conversion: Conversion of Unprotected Aldose Sugars to Polyhydroxyalkyl and *C*-Glycosyl Furans. *ACS Sustainable Chem. Eng.* **2021**, *9*, 11581−11595.
(21) Odoh, S. O.; Cramer, C. J.; Truhlar, D. G.; Gagliardi, L. Quantum-Chemical Characterization of the Properties and Reactivities of Metal-Organic Frameworks. *Chem. Rev.* **2015**, *115*, 6051−6111.
(22) Rogge, S. M. J.; Bavykina, A.; Hajek, J.; García, H.; Olivos-Suarez, A. I.; Sepulveda-Escribano, A.; Vimont, A.; Clet, G.; Bazin, P.; Kapteijn, F.; Daturi, M.; Ramos-Fernandez, E. V.; Llabrés i Xamena, F. X.; Van Speybroeck, V.; Gascon, J. Metal-Organic and Covalent Organic Frameworks as Single-Site Catalysts. *Chem. Soc. Rev.* **2017**, *46*, 3134−3184.
(23) McCarver, G. A.; Rajeshkumar, T.; Vogiatzis, K. D. Computational Catalysis for Metal-Organic Frameworks: An Overview. *Coord. Chem. Rev.* **2021**, *436*, 213777.
(24) Yeh, J.-Y.; Li, S.-C.; Chen, C. H.; Wu, K. C.-W.; Li, Y.-P. Quantum Mechanical Calculations for Biomass Valorization over Metal-Organic Frameworks (MOFs). *Chem.—Asian J.* **2021**, *16*, 1049−1056.
(25) Kresse, G.; Furthmüller, J. Efficient Iterative Schemes for Ab Initio Total-Energy Calculations Using a Plane-Wave Basis Set. *Phys. Rev. B: Condens. Matter Mater. Phys.* **1996**, *54*, 11169−11186.
(26) Kresse, G.; Furthmüller, J. Efficiency of Ab-Initio Total Energy Calculations for Metals and Semiconductors Using a Plane-Wave Basis Set. *Comput. Mater. Sci.* **1996**, *6*, 15−50.
(27) Perdew, J. P.; Burke, K.; Ernzerhof, M. Generalized Gradient Approximation Made Simple. *Phys. Rev. Lett.* **1996**, *77*, 3865−3868.
(28) Grimme, S. Semiempirical GGA-type Density Functional Constructed with a Long-Range Dispersion Correction. *J. Comput. Chem.* **2006**, *27*, 1787−1799.
(29) Kresse, G.; Joubert, D. From Ultrasoft Pseudopotentials to the Projector Augmented-Wave Method. *Phys. Rev. B: Condens. Matter Mater. Phys.* **1999**, *59*, 1758−1775.
(30) Dudarev, S. L.; Botton, G. A.; Savrasov, S. Y.; Humphreys, C. J.; Sutton, A. P. Electron-Energy-Loss Spectra and the Structural Stability of Nickel Oxide: An LSDA+U study. *Phys. Rev. B: Condens. Matter Mater. Phys.* **1998**, *57*, 1505−1509.
(31) Fabris, S.; de Gironcoli, S.; Baroni, S.; Vicario, G.; Balducci, G. Taming Multiple Valency with Density Functionals: A Case Study of Defective Ceria. *Phys. Rev. B: Condens. Matter Mater. Phys.* **2005**, *71*, 041102.
(32) Capdevila-Cortada, M.; Łodziana, Z.; López, N. Performance of DFT+U Approaches in the Study of Catalytic Materials. *ACS Catal.* **2016**, *6*, 8370−8379.
(33) Vandichel, M.; Hajek, J.; Ghysels, A.; De Vos, A.; Waroquier, M.; Van Speybroeck, V. Water Coordination and Dehydration Processes in Defective UiO-66 Type Metal Organic Frameworks. *CrystEngComm* **2016**, *18*, 7056−7069.
(34) Monkhorst, H. J.; Pack, J. D. Special Points for Brillouin-zone Integrations. *Phys. Rev. B* **1976**, *13*, 5188−5192.
(35) Henkelman, G.; Jónsson, H. Improved Tangent Estimate in the Nudged Elastic Band Method for Finding Minimum Energy Paths and Saddle Points. *J. Chem. Phys.* **2000**, *113*, 9978−9985.
(36) Heyden, A.; Bell, A. T.; Keil, F. J. Efficient Methods for Finding Transition States in Chemical Reactions: Comparison of Improved Dimer Method and Partitioned Rational Function Optimization Method. *J. Chem. Phys.* **2005**, *123*, 224101.
(37) Frequencies below 200 cm^{-1} were replaced by 200 cm^{-1} for species to avoid spurious errors when computing Gibbs energies.
(38) Bo, C.; Maseras, F.; López, N. The Role of Computational Results Databases in Accelerating the Discovery of Catalysts. *Nat. Catal.* **2018**, *1*, 809−810.
(39) Alvarez-Moreno, M.; De Graaf, C.; López, N.; Maseras, F.; Poblet, J. M.; Bo, C. Managing the Computational Chemistry Big Data Problem: the ioChem-BD Platform. *J. Chem. Inf. Model.* **2015**, *55*, 95−103.
(40) ioChem-BD Database. https://iochem-bd.bsc.es/browse/handle/100/200147. DOI: 10.19061/iochem-bd-6-116.
(41) Cavka, J. H.; Jakobsen, S.; Olsbye, U.; Guillou, N.; Lamberti, C.; Bordiga, S.; Lillerud, K. P. A New Zirconium Inorganic Building Brick Forming Metal Organic Frameworks with Exceptional Stability. *J. Am. Chem. Soc.* **2008**, *130*, 13850−13851.
(42) Vandichel, M.; Hajek, J.; Vermoortele, F.; Waroquier, M.; De Vos, D.; Van Speybroeck, V. Active Site Engineering in UiO-66 Type Metal-Organic Frameworks by Intentional Creation of Defects: A Theoretical Rationalization. *CrystEngComm* **2015**, *17*, 395−406.
(43) Canivet, J.; Vandichel, M.; Farrusseng, D. Origin of Highly Active Metal-Organic Framework Catalysts: Defects? Defects! *Dalton Trans.* **2016**, *45*, 4090−4099.
(44) Ling, S.; Slater, B. Dynamic Acidity in Defective UiO-66. *Chem. Sci.* **2016**, *7*, 4706−4712.

https://doi.org/10.1021/acssuschemeng.1c08021
ACS Sustainable Chem. Eng. 2022, 10, 3567−3573

(45) Gonell, F.; Boronat, M.; Corma, A. Structure-Reactivity Relationship in Isolated Zr Sites Present in Zr-Zeolite and ZrO_2 for the Meerwein-Ponndorf-Verley Reaction. *Catal. Sci. Technol.* **2017**, *7*, 2865−2873.
(46) Hajek, J.; Vandichel, M.; Van de Voorde, B.; Bueken, B.; De Vos, D.; Waroquier, M.; Van Speybroeck, V. Mechanistic Studies of Aldol Condensations in UiO-66 and UiO-66-NH_2 Metal Organic Frameworks. *J. Catal.* **2015**, *331*, 1−12.
(47) Caratelli, C.; Hajek, J.; Cirujano, F. G.; Waroquier, M.; Llabrés i Xamena, F. X.; Van Speybroeck, V. Nature of Active Sites on UiO-66 and Beneficial Influence of Water in the Catalysis of Fischer Esterification. *J. Catal.* **2017**, *352*, 401−414.
(48) Ortuño, M. A.; Bernales, V.; Gagliardi, L.; Cramer, C. J. Computational Study of First-Row Transition Metals Supported on MOF NU-1000 for Catalytic Acceptorless Alcohol Dehydrogenation. *J. Phys. Chem. C* **2016**, *120*, 24697−24705.
(49) Sittiwong, J.; Boonmark, S.; Nunthakitgoson, W.; Maihom, T.; Wattanakit, C.; Limtrakul, J. Density Functional Investigation of the Conversion of Furfural to Furfuryl Alcohol by Reaction with *i*-Propanol over UiO-66 Metal-Organic Framework. *Inorg. Chem.* **2021**, *60*, 4860−4868.
(50) Valekar, A. H.; Lee, M.; Yoon, J. W.; Kwak, J.; Hong, D.-Y.; Oh, K.-R.; Cha, G.-Y.; Kwon, Y.-U.; Jung, J.; Chang, J.-S.; Hwang, Y. K. Catalytic Transfer Hydrogenation of Furfural to Furfuryl Alcohol under Mild Conditions over Zr-MOFs: Exploring the Role of Metal Node Coordination and Modification. *ACS Catal.* **2020**, *10*, 3720−3732.
(51) Kim, M.; Cahill, J. F.; Fei, H.; Prather, K. A.; Cohen, S. M. Postsynthetic Ligand and Cation Exchange in Robust Metal-Organic Frameworks. *J. Am. Chem. Soc.* **2012**, *134*, 18082−18088.
(52) Lee, Y.; Kim, S.; Kang, J. K.; Cohen, S. M. Photocatalytic CO_2 Reduction by a Mixed Metal (Zr/Ti), Mixed Ligand Metal-Organic Framework Under Visible Light Irradiation. *Chem. Commun.* **2015**, *51*, 5735−5738.
(53) Lammert, M.; Wharmby, M. T.; Smolders, S.; Bueken, B.; Lieb, A.; Lomachenko, K. A.; De Vos, D.; Stock, N. Cerium-Based Metal Organic Frameworks with UiO-66 Architecture: Synthesis, Properties and Redox Catalytic Activity. *Chem. Commun.* **2015**, *51*, 12578−12581.
(54) Momeni, M. R.; Cramer, C. J. Computational Screening of Roles of Defects and Metal Substitution on Reactivity of Different Single- vs Double-Node Metal-Organic Frameworks for Sarin Decomposition. *J. Phys. Chem. C* **2019**, *123*, 15157−15165.
(55) Saraci, F.; Quezada-Novoa, V.; Donnarumma, R.; Howarth, A. J. Rare-Earth Metal-Organic Frameworks: From Structure to Applications. *Chem. Soc. Rev.* **2020**, *49*, 7949−7977.
(56) Vitillo, J. G.; Lu, C. C.; Cramer, C. J.; Bhan, A.; Gagliardi, L. Influence of First and Second Coordination Environment on Structural Fe(II) Sites in MIL-101 for C-H Bond Activation in Methane. *ACS Catal.* **2021**, *11*, 579−589.
(57) Wei, R.; Gaggioli, C. A.; Li, G.; Islamoglu, T.; Zhang, Z.; Yu, P.; Farha, O. K.; Cramer, C. J.; Gagliardi, L.; Yang, D.; Gates, B. C. Tuning the Properties of Zr_6O_8 Nodes in the Metal Organic Framework UiO-66 by Selection of Node-Bound Ligands and Linkers. *Chem. Mater.* **2019**, *31*, 1655−1663.
(58) Feng, X.; Hajek, J.; Jena, H. S.; Wang, G.; Veerapandian, S. K. P.; Morent, R.; De Geyter, N.; Leyssens, K.; Hoffman, A. E. J.; Meynen, V.; Marquez, C.; De Vos, D. E.; Van Speybroeck, V.; Leus, K.; Van Der Voort, P. Engineering a Highly Defective Stable UiO-66 with Tunable Lewis-Brønsted Acidity: The Role of the Hemilabile Linker. *J. Am. Chem. Soc.* **2020**, *142*, 3174−3183.

https://doi.org/10.1021/acssuschemeng.1c08021
ACS Sustainable Chem. Eng. 2022, 10, 3567−3573